Contents lists available at ScienceDirect

European Journal of Pharmaceutical Sciences

journal homepage: www.elsevier.com

A 3D printed bilayer oral solid dosage form combining metformin for prolonged and glimepiride for immediate drug delivery

Christos I. Gioumouxouzis[a], Apostolos Baklavaridis[b], Orestis L. Katsamenis[c], Catherine K. Markopoulou[a], Nikolaos Bouropoulos[d, e], Dimitrios Tzetzis[f], Dimitrios G. Fatouros[a, *]

[a] Laboratory of Pharmaceutical Technology, Department of Pharmaceutical Sciences, Aristotle University of Thessaloniki, GR-54124 Thessaloniki, Greece
[b] Department of Mechanical and Industrial Design Engineering, TEI of Western Macedonia, Kozani, Greece
[c] University of Southampton, μ-VIS X-Ray Imaging Centre, Faculty of Engineering and the Environment, SO17 1BJ Southampton, UK
[d] Department of Materials Science, University of Patras, 26504 Rio, Patras, Greece
[e] Foundation for Research and Technology Hellas, Institute of Chemical Engineering and High Temperature Chemical Processes, Patras, Greece
[f] International Hellenic University, School of Science and Technology, 14km Thessaloniki - N. Moudania, Thermi GR57001, Greece

ARTICLE INFO

Keywords:
Fused deposition modelling
3D printing
Metformin
Glimepiride
Bilayer dosage form
Mechanical properties
Micro-computer tomography

ABSTRACT

Fused Deposition Modelling (a.k.a. FDM-3D printing) has been previously employed in the development of personalized medicines with unique properties and release behavior. In the present work, a bilayer dosage form containing two anti-diabetic drugs with different daily dosage regimens; i.e. metformin and glimepiride, was manufactured via FDM 3D printing, studied using a variety of techniques and characterized in vitro. Metformin and glimepiride were embedded in Eudragit® RL sustained release layer and polyvinyl alcohol (PVA) layer respectively. Incorporation of more than one API's into the formulation is desirable, as it increases patient compliance and reduces cost of treatment, especially when distinct dosages of API's can be adjusted individually in situ, in order to meet each patient's specific needs, a capability provided by 3D printing. A number of different preparation methods, which involved different plasticizers and extruders, were tested on manufacturing Eudragit® RL drug-loaded filaments for printing the sustained release layer. The properties of the produced filaments were assessed by means of mechanical and physicochemical characterization techniques and the filaments with the optimum properties were used for printing. Microfocus computed tomography (μCT) imaging-based actual/nominal comparison analysis showed a printing accuracy ranging between −100, +200 μm, while X-ray (XRD) diffractograms revealed the incorporation of the (initially crystalline) API's as amorphous dispersions into polymer matrices. Dissolution tests showed sufficient drug release for both drugs in desired time frames (75 min for glimepiride and 480 min for metformin). The results from the current study emphasize the potentiality of 3D printing technology for tailor-made solid dosage forms for combined pharmacotherapy, even at the cases when API's with different desirable release profiles are employed.

1. Introduction

Fusion Deposition Modelling (FDM) 3D printing is a technique that creates solid objects by successive deposition of strands of molten polymers via the nozzle of a moving printhead. In pharmaceutics FDM 3D printing has been employed in the creation of dosage forms with elaborate shapes (Goyanes et al., 2015c), dosage forms that exhibit specific release characteristics (Chai et al., 2017; Gioumouxouzis et al., 2017; Goyanes et al., 2015b; Okwuosa et al., 2016a; Pietrzak et al., 2015), personalized implants (Boetker et al., 2016; Genina et al., 2016; Holländer et al., 2016; Zhang et al., 2017) and 3D printed matrices used as carriers or substrates for other drug loaded release devices (Beck et al., 2017; Maroni et al., 2017; Melocchi et al., 2015; Sandler et al., 2014). The introduction of 3D printers with dual printheads allowed fabrication of even more sophisticated dosage forms, that could modify and regulate the release of the incorporated API's, relying on their elaborate design (Gioumouxouzis et al., 2017; Goyanes et al., 2015d; Okwuosa et al., 2016a). Attempts had also been made to use FDM 3D printing at lower temperatures, increasing the range of possible API's that can be formulated using that technique (Okwuosa et al., 2016b; Sadia et al., 2016).

* Corresponding author.
Email address: dfatouro@pharm.auth.gr (D.G. Fatouros)

https://doi.org/10.1016/j.ejps.2018.04.020
Received 5 January 2018; Received in revised form 15 April 2018; Accepted 16 April 2018
Available online xxx
0928-0987/

Incorporation of more than one API's with different release patterns in one dosage form (a beneficial approach, as it reduces frequency of medication intake and improves patience compliance) (Paes et al., 1997), was previously investigated using different 3D printing techniques (semisolid extrusion 3D printing) (Khaled et al., 2015a, 2015b). In the current study we attempted to create such formulations using FDM 3D printing, by not relaying to the modified release of different API's from a particular polymer matrix due to morphological characteristics of the 3D printed dosage form (Goyanes et al., 2015d), but also incorporating different API's into separate polymer carriers with distinct release characteristics.

For that purpose, two commonly co-prescribed drugs used in the treatment of type II diabetes (metformin and glimepiride) were investigated as model-drugs. This choice was rationalized from the fact that the co-administration of these API's posed major challenges, as their dosage regimen is different (once daily for glimepiride, 2–3 times daily for metformin) (Hwang et al., 2013), their daily dosing differs by two orders of magnitude (1–4 mg for glimepiride, 500–1000 mg for metformin) ("BNF", 2014) and they are absorbed at different sites of the GI tract (mainly at gastric environment for glimepiride and small intestine for metformin – small amounts of metformin are also absorbed in the stomach or large intestine) (McCreight et al., 2016; Ning et al., 2011). To overcome these challenges a bilayer design was preferred, consisting of a metformin-loaded Eudragit® RL layer for prolonged release and a glimepiride-loaded PVA layer for immediate release.

Additionally, the very high dosing of metformin itself posed a major challenge, as previous studies have shown that incorporation of high quantities of API's deteriorate the quality of the drug-loaded filament used to feed the 3D printer (Goyanes et al., 2015d). Therefore, filament production was investigated by using and evaluating a variety of plasticizers (citric acid monohydrate, triethyl citrate (TEC), PEG 400) and employing two different Hot-Melt extruders (twin-screw and single screw). Mechanical properties of the produced filaments were evaluated, as only Hot-melt Extrusion (HME) produced filaments with adequate hardness and elasticity are printable using FDM 3D printers (Zhang et al., 2017).

Additionally, one of the (secondary) aims of the study was the evaluation of different compounds (mainly plasticizers) in filament production.

An alternative technique for the determination of the mechanical properties of polymer blends is the instrumented indentation technique, which was utilized in the current work. This is a simple but powerful testing technique, which can provide useful information about the mechanical properties of polymers. Various studies have compared the results obtained from such techniques with the results obtained from the traditional tensile tests especially for the elastic modulus calculation (Mansour et al., 2013; Mansour and Tzetzis, 2013; Tzetzis et al., 2013). It is anticipated that in the near future, these techniques will also be attractive in the pharmaceutical industry and especially for the evaluation of 3D printing materials, due to the simplicity and practicality of the experiments involved. Such techniques, apart from the localized characterization of the material, might be also crucial in the study of the bulk material elastic properties through multiple measurements, if their results are averaged through computational methods.

μCT has been previously employed in the qualitative evaluation of 3D printed dosage forms (Gioumouxouzis et al., 2017) and the quantitative evaluation of 3D printed scaffolds used as carriers of self-emulsifying drug delivery systems (Markl et al., 2017). In the present work, it is attempted to quantitative evaluate the printing accuracy and internal morphology of a 3D printed API-loaded dosage forms by utilizing that imaging technique enabling the creation of solid dosage forms for personalized medicine.

Summarizing, in the present work we attempted to demonstrate the feasibility of creating personalized dosage forms that incorporate more than one API's, loaded into different polymeric carriers. Varying properties of the carriers would allow the simultaneous usage of API's that are normally administered at different times during the day, in all-in-one formulations, created for each individual patient in accordance to his specific needs. To achieve this goal a detailed understanding of the behavior of filaments used for 3D printing, as also of the morphology of 3D printed dosage forms is mandatory, therefore employment of sophisticated evaluation techniques, i.e. μCT and instrumented indentation was deemed necessary.

2. Materials and methods

2.1. Materials

Glimepiride (MW: 490.616, water solubility at 25 °C 2.7×10^{-4} mg/mL at 25 °C) (Ning et al., 2011) and partially hydrolyzed PVA (Mowiol® 4–88, MW ~31.000), were purchased from Sigma-Aldrich, MI, USA. Metformin HCl (MW: 129.162, water solubility at 25 °C 100 mg/mL at 25 °C) (Cheng et al., 2004) and Mannitol (MW: 182.17, water solubility at 37 °C: 193.5 g/L) (Yalkowsky et al., 2010) were purchased from Fagron Hellas, Greece. Eudragit® RL PO was kindly offered from Evonik AG, Germany. Calcium stearate was purchased from Caelo, Germany, PLA (Resomer® L 210 S) from Boehringer-Ingelheim, Germany, PEG 400 from Syndesmos SA, Greece and PLA filament (1.75 mm diameter, print temperature 180–220 °C, density 1.24 g/mL) from FormFutura VOF, The Netherlands. Salts, used for the preparation of the dissolution medium and HPLC mobile phases, were of analytical grade and purchased from Merck, Germany (KH_2PO_4) and Panreac, Spain (NaH_2PO_4 and $NH_4H_2PO_4$). ACN and H_2O of the mobile phases were HPLC grade and also purchased from Sigma-Aldrich, MI, USA.

2.2. Preparation of drug-loaded filament

2.2.1. Preparation of metformin-loaded Eudragit® filament

In order to create sustained release metformin-loaded filament, several formulations (summarized in Table 1) were tested, containing mainly metformin and Eudragit® RL PO. An array of plasticizers was also tested (PEG 400, TEC, citric acid monohydrate) in concentrations previously employed for polymer plasticization (Maroni et al., 2017; Pietrzak et al., 2015; Schilling et al., 2008), whereas PLA was added in selected formulations to improve mechanical strength of the fila-

Table 1
% composition of tested filament formulations.

Compound	1	2	3	4	5	6	7
Metformin	50	50	50	50	50	50	50
Eudragit® RL PO	35	40	45	45	35	35	35
PLA (Resomer®)	–	–	–	–	8	10	–
PLA filament (granulated)	–	–	–	–	–	–	10
TEC	–	–	5	–	–	–	–
CA monohydrate	15	10	–	–	–	–	–
PEG 400	–	–	–	5	7	5	5

ment. Calcium stearate was not used in this case, since die swell of the extrudate was not excessive and could be overcome by using extrusion nozzles with smaller diameter. The total amount of excipients and API's used in each batch was 50 g.

For the extrusion of these mixtures a Filabot Original® single-screw extruder (Filabot Inc., VT, USA) was utilized. The extruder was operated at 35 rpm and the mixtures were extruded at 140 °C through a 1.75 mm nozzle. The filament that presented the optimum mechanical properties derived from the mixture that contained 50% metformin, 35% Eudragit® RL PO, 10% powderized PLA filament and 5% PEG 400 (Form. 7b) and was used for the preparation of 3D printed dosage forms.

The formulation that resulted in optimum filament was also extruded using a co-rotating twin-screw HAAKE MiniLab® extruder (Thermo Scientific, MA, USA), operating in nitrogen environment and extruding via a 1.5 mm nozzle, after 5 min of homogenization inside the heated barrel. The extrusion temperature was set at 157 °C and the screw speed at 23 rpm (Form. 7a).

2.2.2. Preparation of glimepiride-loaded PVA filament

Mowiol® 4–88 (PVA) and mannitol were chosen based on their properties. Partially hydrolyzed Mowiol® 4–88 dissolves rapidly at 40 °C (Clariant, 1999), whereas mannitol (used as plasticizer (Aydin and Ilberg, 2016)) is less hygroscopic compared to other sugars (e.g. sorbitol) (Gombás et al., 2003). Calcium stearate was added to prevent excessive die swell and facilitate extrusion (Seymour, 1990).

24 g of Mowiol® 4–88 were grinded using a grinder and sieved through a 600 μm mesh. Mowiol® 4–88, 4.5 g mannitol, 0.9 mg calcium stearate and 0.6 mg glimepiride were subsequently mixed in a mortar and pestle, until complete homogenization was achieved (mixture composition: 80% PVA, 15% mannitol, 3% calcium stearate and 2% glimepiride, Formulation 8). Subsequently, the homogenized mixture was fed in the aforementioned twin-screw HAAKE MiniLab® extruder, operated at 23 rpm screw speed and equipped with a 1.5 mm custom made nozzle. The filament was extruded at 190 °C (torque 0.07 Nm, pressure 3–7 bar) and stored in a vacuum desiccator to avoid exposure of hygroscopic PVA to moisture.

The composition of the formulations was chosen in an effort to create dosage forms resembling similarities with marketed products. The ratios and the role of the excipients used in the current student have been utilized in previous studies; the amount of plasticizers used was the adequate to achieve plasticization, as referred in relevant literature (Pietrzak et al., 2015; Schilling et al., 2008; Maroni et al., 2017). The only compound arbitrary chosen was PLA, in relatively small amount that would not reduce excessively the amount of Eudragit used.

2.3. Mechanical properties testing (Dynamic Micro-Indentation Test)

In an attempt to ensure the smooth operation of the FDM feeding gear the suitability of the produced filaments was evaluated by means of Dynamic Micro-Indentation Test.

A detailed investigation of the mechanical behavior of the compounds in a filament form was performed using a dynamic ultra-micro-hardness tester (DUH-211; Shimadzu Co., Kyoto, Japan) fitted with a triangular pyramid indenter tip (Berkovich indenter). The specimens were fixed onto an attached holder. Dynamic micro-indentation mainly involves applying a controlled load (P) through a diamond tip that is in contact with a surface. The penetration depth (h) of indentation is continuously recorded as a function of load. Fig. 1A shows a schematic illustration of the typical micro-indentation load–penetration depth curve obtained from Dynamic Micro-Indentation Tests. During indenter loading and unloading, the specimen is subjected to both plastic deformation (h_p) and elastic deformation (h_e). The total deformation (h_t) is the sum of h_p and h_e in the micro-indentation load–penetration depth curve. Moreover, the indentation hardness and elastic modulus can be obtained from the indentation load and penetration depth data.

The indentation hardness (H_{it}) of the samples is a measure of the resistance to permanent deformation damage and it was calculated from the following equation:

$$H_{it} = \frac{P_{\max}}{A_p} \quad (1)$$

where P_{max} is the maximum force and A_p is the projected area of contact between the indenter and the sample. A_p is calculated from the following equation:

$$A_p = 23,96\, h_c^2 \quad (2)$$

where h_c is the depth of contact of the indenter with the sample calculated as follows:

$$h_c = h_t - \frac{3}{4}\left(h_t - h_r\right) \quad (3)$$

where h_r is derived from the load-displacement curve and is the intercept of the tangent to the unloading cycle at P_{max} with the displacement axis.

The elastic modulus (E) of the sample was calculated from the following equation:

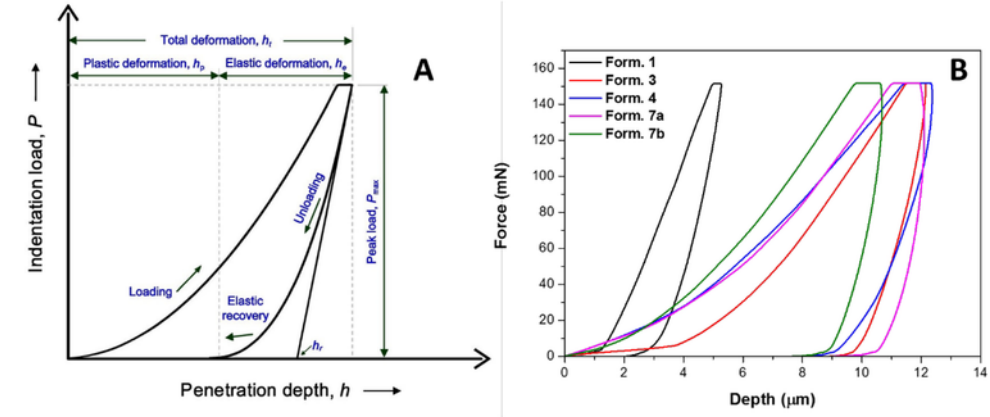

Fig. 1. A. Schematic illustration of a typical micro-indentation load – penetration depth curve, B. Indentation load-penetration depth curves for tested formulations (one representative curve shown for each formulation).

$$\frac{1}{E_r} = \frac{1-\upsilon_s^2}{E_s} + \frac{1-\upsilon_i^2}{E_i} \quad (4)$$

where $E_{i,s,}$ and $\nu_{i,s}$ are the elastic modulus and Poisson's ratio, respectively, for the indenter and the specimen. For a diamond indenter, E_i is 1140 GPa and ν_i is 0.07. For the materials under test a Poisson's ratio of 0.4 was assumed for the calculations.

In this study, the Dynamic Micro-Indentation Test was carried out with peak loads (P_{max}) of 150 mN. The load rate was kept constant at 13.324 mN/s, and the hold time at the maximum load was set to 3 s. The dynamic micro-indentation results, such as indentation hardness and elastic modulus, were obtained as the average value of five measurements.

2.4. Determination of drug loading

2.4.1. Glimepiride drug-loading determination

10 mg of glimepiride were dissolved in 50 mL methanol, creating a 200 mg/L stock solution. That solution was utilized to create five solutions (using water, with its pH adjusted to 7.8, as a diluent), that were used to obtain a reference curve. pH was raised to 7.8 (using KH_2PO_4/NaOH buffer) because glimepiride solubility is pH-dependent and raises rapidly above pH 7.5 (Ning et al., 2011).

Subsequently, filament pieces weighting 300 mg were dissolved in 50 mL of distilled water (pH 7.8) following bath sonication. Pieces (at least three for every filament tested) were chosen from different spots of the filament coil, to ensure uniform distribution of glimepiride in the entire filament. 3 mL of these solutions were transferred to 25 mL volumetric flasks and after that dilution, solutions were filtered with Millipore® Millex–HV PVDF 0.45 μm filters (Merck, Germany). The filtrate was used to determine glimepiride concentration, by employing a UV-2501PC spectrophotometer (Shimadzu, Japan) operating at 228 nm.

2.4.2. Metformin drug-loading determination

A similar procedure to the one employed for the determination of glimepiride drug loading was used. The two differences are, that the filaments were powdered to ensure that all metformin incorporated in the filament would be acquired (as Eudragit® RL is insoluble in water) and the usage of pH 6.8 KH_2PO_4/NaOH buffer solution as a solvent. Reference curve solutions were prepared and the obtained curve was used to determine metformin drug loading in filament sample solutions, using a UV detector at 232 nm.

2.5. Preparation of 3D printed formulations

3D printed dosage forms were designed using AutoCAD 2016® (Autodesk Inc., USA) (Fig. 2A). Templates were exported as stereolithography (.stl) files to Makerware® software version 3.9.2 (MakerBot Inc., USA), (Fig. 2B). The preferred design was flat cylindrical with smoothed edges (pill- shaped), consisting of two layers, an upper layer of water-soluble glimepiride-loaded PVA and a lower metformin-loaded sustained release layer, composed of the above described filaments. That shape was chosen for both patience compliance (especially for large dosage forms) and construction simplification, as it involves only one nozzle switching during printing, improving reproducibility and eliminating printing defects.

2.5.1. Calculations for 3D formulations' dimensions

The dimensions of the 3D printed dosage forms were calculated considering the target of 2 mg glimepiride and 500 mg metformin present in a marketed product (Amaryl-M® 2/500 mg, Sanofi, France).

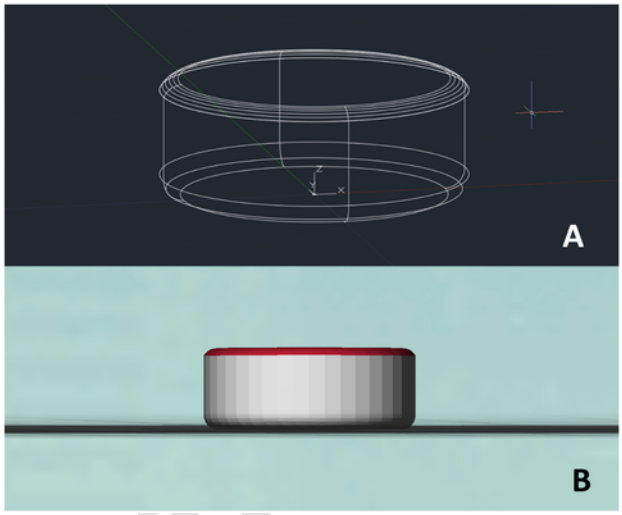

Fig. 2. A. Autocad® draw of 3D printed dosage form, B. stereolithography (.stl) model of 3D printed dosage form.

2.5.1.1. Upper glimepiride-loaded immediate release layer In a previous work (Gioumouxouzis et al., 2017), it was demonstrated that 3D printing often results in structures that are not absolutely solid, but incorporate small internal voids and pores. This may result in mass deviations from the desired values, if the calculation of dimensions relies on theoretical density values or even filament measured density. To overcome this, mass (m) was expressed as a function of only one dimension (height - h) of the 3D printed formulation (keeping other dimensions constant) and a liner equation between these two parameters was established, by printing and weighting dosage forms with different heights (Pietrzak et al., 2015).

Specifically, cylinder volume's formula is

$$V_c = \pi r_c^2 h_c \quad (5)$$

(h_c = cyl. height, r_c = cyl. radius) and also

$$m = \rho * V \quad (6)$$

(ρ = density).

Combining Eqs. (5) and (6) results in

$$m_c = \pi \rho r_c^2 h_c. \quad (7)$$

By keeping r_c constant (π and ρ values are also constant) a linear y = ax + b relation is deduced.

If r_c is set to be 7.5 mm, that relation in the case of glimepiride-loaded PVA layer corresponds to equation:

$$m_g = 208.73 h_g - 151.76 \ \left[R^2 = 0.981\right], \quad (8)$$

(m_g = glimepiride layer mass and h_g = glimepiride layer height).

The establishment of the above equation, was based on printing and weighting 5 single-layer dosage forms with different heights.

Considering that the filament contains 2% w/w glimepiride, the desired filament mass should be adjusted to m_g = 100 mg. Glimepiride-loaded PVA filament was found to contain 89.49% of the theoretically incorporated glimepiride, therefore, the theoretical value of 2 mg of glimepiride could be achieved with an upper PVA layer weighting 111.74 mg. Eventually, by using Eq. (8) the desired height for the upper glimepiride-loaded PVA layer is h_g = 0.552 mm.

2.5.1.2. Lower metformin-loaded sustained release layer In this case, two different filaments were utilized, one deriving from the twin-screw and the other from the single-screw extruder. So, for the first extruder Eq.

(7) is transformed into:

$$m_{mT} = 208.73h_{mT} - 151.76 \ \left[R^2 = 0.984\right], \quad (9)$$

if r_c is set to be 7.5 mm (m_m = metformin layer mass and h_m = metformin layer height) and for the second extruder Eq. (7) is transformed into:

$$m_{mS} = 191.47h_{mS} - 12.877 \ \left[R^2 = 0.962\right], \quad (10)$$

if r_c is set to be 7.5 mm, using the aforementioned printing and weighting method.

Considering that the filament contains 50% w/w metformin, the desired filament mass should be adjusted to $m_m = 1000$ mg. Metformin-loaded filament was found to contain 99.53% of the theoretically incorporated metformin, corresponding to an upper PVA layer of 1004.72 mg. Eventually, by using Eq. (9) the desired height for the lower metformin-loaded Eudragit® layer is $h_{mT} = 5.54$ mm and by using Eq. (10) is $h_{mS} = 5.18$ mm.

2.5.2. Printing conditions

Printing was performed in a MakerBot Replicator® 2× 3D printer (MakerBot Inc., NY, USA), using the first nozzle for printing metformin-loaded lower layer and the second nozzle for printing PVA glimepiride-loaded upper layer. The following settings were employed:

i) *Eudragit®-metformin layer printing nozzle*: $T_{print} = 170$ °C, $T_{platform} = 90$ °C, infill = 100%, layer height = 0.2 mm, printing speed = 70 mm/s, travel speed = 90 mm/s, number of shells = 2.

ii) *Glimepiride-PVA layer printing nozzle*: $T_{print} = 205$ °C, $T_{platform} = 90$ °C, infill = 100%, layer height = 0.2 mm, printing speed = 70 mm/s, travel speed = 90 mm/s, number of shells = 2.

Raft and purging walls options were deactivated.

To facilitate 3D printing the following modifications were employed:

i) Building plate was covered with Blue painter's tape (3 M, MI, USA) to ensure proper adhesion of the Eudragit®-based lower layer to the printing surface.
ii) Printhead's feeding barrel was lubricated using oleic acid (Sigma Aldrich, MI, USA -technical grade, 90%), approximately every 10 printings, in order to avoid jamming, caused by high friction between Eudragit®-metformin filament and barrel walls.

The dimensions of the produced 3D printed formulations were measured using an electronic micrometer and finally, formulations were weighted and stored in a vacuum desiccator as well.

2.6. Physical characterization

2.6.1. Thermal analysis studies

Differential scanning calorimetry (DSC) was employed to analyze thermal behavior of materials used, utilizing a 204 F1 Phoenix DSC calorimeter (Netzsch GmBH, Germany). 5 mg of raw materials and samples, as also samples from drug-loaded filaments and drug-loaded upper and lower layers from 3D printed formulations, were loaded on aluminum plates and their DSC profiles were acquired from 30 °C to 350 °C, at a heating rate of 10 °C/min. The measurements were conducted in nitrogen environment (flow: 70 mL/min). The software used for DSC measurements was Proteus ver. 5.2.1 (Netzsch GmBH, Germany).

The thermal decomposition of the samples was assessed by thermogravimetric analysis (TGA). 10 mg of tested formulations and starting materials were placed in a platinum pan and heated from 35 to 500 °C at a rate of 10 °C/min under an air atmosphere (40 mL/min) using a TA Q500 Thermogravimetric Analyzer (TA Instruments, New Castle, DE, USA).

2.6.2. X-ray powder diffraction (XRD) studies

The crystallinity of raw materials and produced printed formulations was investigated by means of XRD. X-ray diffractograms were obtained using a powder X-ray diffractometer, D8-Advance (Bruker, Germany) with Ni-filtered $CuKa_1$ radiation ($\lambda = 0.154059$ nm), operated at 40 kV and 40 mA. Samples were scanned from 2Theta = 5 to 50 at a step of 0.02° and a scan speed of 0.35 s/step.

2.7. Morphological characterization

2.7.1. Macroscopic and volumetric evaluation of the printed dosage forms

Dimensions of 3D printed dosage forms were measured using a Kreator digital caliper (Varo, Belgium) and their images were acquired using an Ixus 1000 HS (Canon, Japan) camera.

In addition to that, the accuracy of the printing was assessed by means of μCT by comparing the 'nominal' shape (i.e. the designed model) to the 'actual' printed object. For this, a randomly selected specimen was selected and imaged using a Zeiss 160 kVp Versa 510 μCT scanner. Imaging conditions were selected so that a minimum of 10% transmission of the incoming X-ray beam was preserved at all exposed angles while contrast between the two materials of interest (PVA and Eudragit®) maintained at satisfactory levels. The scan was conducted at a peak voltage of 80 kVp and the beam was pre-filtered using 1 mm of SiO_2. To achieve sufficient flux, the power of the filament was 7 W (87.5 μA). The 2026 × 2026 pixels detector was used un-binned and the source to detector distance was set to 128 mm (SrcZ: −33, DetZ: +95), which in combination with the 0.4× lens resulted in a pixel size of 8.93 μm; i.e. a spatial resolution of approximately 20–25 μm. During the tomogram, a total of 4001 radiographs were collected with an angular step of c. 0.09° over a 360-degree rotation of the sample. Following the acquisition, the raw data were reconstructed using Zeiss' reconstruction software, which uses a filtered back projection algorithm, and exported as a 16-bit tiff-stack for visualization and analysis.

Visualization and analysis of the μCT data was conducted using Volume Graphics VGStudioMAX. The actual-nominal comparison analysis comprised of a [a] semi-automatic segmentation of the additive manufactured object using a combination of thresholding, magic wand tool and manual drawing/cleaning of misclassified areas, [b] determination of an isosurface of the segmented regions of interest (ROIs) that included all the segmented pixels, [c] mesh generation based on the determined isosurface, [d] import of the CAD design in the form of .stl and [e] registration of the generated mesh model to the imported CAD design. Finally, porosity analysis was conducted on 16.99 mm^3 (253 × 253 × 251 voxels) central sub-volume in Fiji/ImageJ (Schindelin et al., 2012; Schneider et al., 2012).

2.7.2. Microscopic evaluation (scanning electron microscopy studies)

The morphological features of the extruded filaments, as well as those of the 3D printed tablet, were assessed using a Zeiss SUPRA 35VP SEM microscope. Samples were placed on aluminum stubs and coated with 15 nm gold, using an Emitech K550X DC sputter coater (Emitech Ltd. Ashford, Kent, UK) apparatus, prior to imaging.

2.8. Dissolution studies

The dissolution experiments of the bilayer dosage forms were performed using a USP dissolution paddle apparatus (PT-DT7 Pharma Test AG, Germany) at 75 rpm. pH of the dissolution medium was adjusted at 7.8 in accordance to FDA and British Pharmacopoeia specifications, to improve glimepiride solubility, using the suggested KH_2PO_4/NaH_2PO_4 buffer ("Dissolution Methods", n.d.; Stationery Office (Great Britain),

2016). All the experiments were performed at least in triplicate. Samples were taken at pre-determined time points for 9 h (every 15 min for the first 75 min and every 1 h after 120 min), centrifuged in a Heraeus Labofuge® 400R centrifuge (Thermo Scientific, MA, USA) for 15 min at 4500 rpm, filtered using Millipore® Millex–HV PVDF 0.45 μm filters (Merck, Germany) and analyzed by means of HPLC.

High metformin loading, made metformin samples dilution mandatory. In this case glimepiride concentrations dropped below LOQ, making simultaneous determination of the two API's impossible. As a result, two separate HPLC assays were employed to analyze metformin and glimepiride samples. Metformin determination assay consisted of an Agilent Zorbax® 300-SCX column 250×4.6 mm i.d., 5 μm, using a mobile phase composed of 1.7% $NH_4H_2PO_4$ buffer pH 3.0:acetonitrile (70:30 v/v), with flow rate 1.0 ml min^{-1}, inj. volume 20 μL and detector wavelength 232 nm (Pawar et al., 2008). Dissolution samples were diluted at a 1:10 rate, resulting in solutions with concentrations between 5 and 50 μg/mL, where reference curve indicated excellent linearity ($R^2 = 0.999$).

Glimepiride determination assay consisted of a Supelco Ascentis® C8 column 150×4.6 mm i.d, 5 μm, using a mobile phase composed of KH_2PO_4 buffer pH 3.0:acetonitrile (40:60 *v/v*), with flow rate 1.0 ml min^{-1}, inj. Volume 20 μL and detector wavelength 228 nm (Ramesh and Habibuddin, 2014). Glimepiride content of dissolution samples ranged between 0.5 and 2 μg/ml, where corresponding reference curve showed also excellent linearity ($R^2 = 0.999$).

3. Results and discussion

Hot-melt extrusion of all mixtures was feasible, although HAAKE MiniLab® twin-screw extruder required higher temperatures (~20 °C) to extrude the same mixtures in comparison to Filabot® single-screw extruder. This could be attributed to the larger screw size of the single screw extruder (HAAKE: Screw diameter: conical 5/14 mm, Screw length: 109.5 mm – Filabot: Screw diameter: 16 mm, Screw length: 195.58 mm), that resulted in development of higher pressures inside the heated barrel, facilitating extrusion at temperatures slightly lower than the melting temperatures of the compounds (semi-solid state) (Abeykoon et al., 2011; Rauwendaal, 2014).

Despite higher temperatures, no discoloration was observed in twin-screw extruder, probably due to shorter residence of the mixture inside the heated barrel and the nitrogen environment involved. On the contrary, filaments produced from single screw extruder exhibited different degrees of color change, ranging from slight graying in the case of formulations 5 to 7, to complete browning in formulations 1 and 2 (probably attributed to decomposition of the citric acid monohydrate contained in these formulations). In Fig. 3 images of the produced filaments are presented.

Dynamic Micro Hardness test results are presented in Fig. 4. Typical indentation load–penetration depth curves of the various filament formulations are shown in Fig. 1B. The indentation load-penetration depth curves were obtained during indenter loading and unloading. However, measurements for compounds 5 and 6 were not feasible,

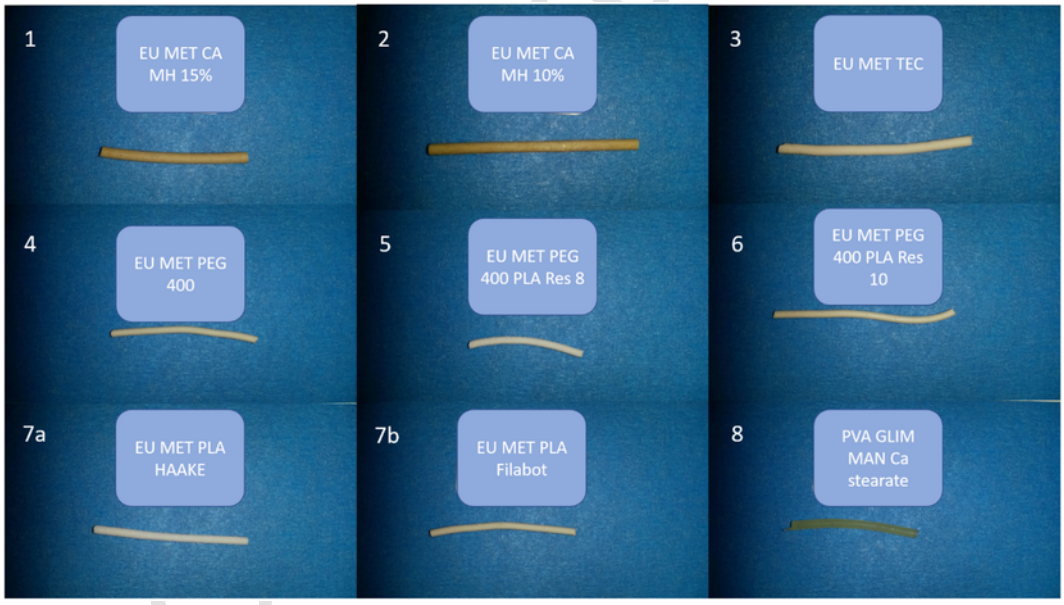

Fig. 3. Images of the HME produced filaments of the tested formulations. Image numbers correspond to formulation numbers.

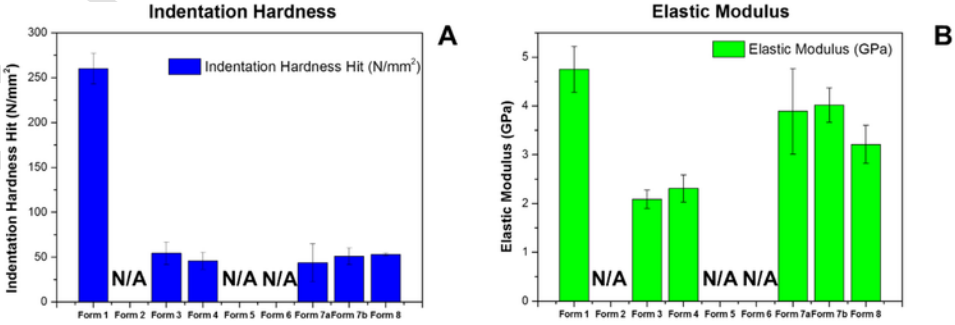

Fig. 4. A. Indentation Hardness and B. Elastic Moduli of filaments of tested formulations using Dynamic Micro Hardness Tester.

since the material was excessively soft not allowing the instrument to take any indentation-resistance measurements. Fig. 4A and B summarizes the indentation harnesses and elastic moduli of the various compound materials under study. The values of the indentation hardness and elastic modulus of formulation 1 were higher than the other materials under study. Such values indicate the fact that the fabricated filament was extremely brittle and it was not possible to proceed with any 3D printing operation. Measurements for formulation 2 were avoided since only lowering the percentage of CA monohydrate to 10% would reveal similar results. Formulation 3 and 4 compounds revealed similar properties regarding the two essential mechanical properties, i.e. the indentation hardness and the elastic modulus. The elastic modulus was 2.09 GPa and 2.31 GPa for the compound 3 and 4 respectively, with values within their standard deviations. Although both materials exhibited improved printability in comparison to formulation 1, they resulted in very frequent unsuccessful printing. Formulation 7a and 7b compounds (which were essentially the same material) showed almost identical elastic moduli having values of 3.89 GPa and 4,02 GPa, meaning that the type of filament extruder (twin screw and single screw) played a minor role in the mixing of the formulations. Both types of filaments provided excellent 3D prints. Formulation 8 (PVA-based) equally provided excellent prints and its elastic modulus was measured to be 3.21 GPa, which is close to the values obtained for formulations 7a and 7b. It seems that for such materials, the elastic modulus should be in the range of 3 to 4 GPa in order the filament to be 3D printable. These elastic moduli values are almost double the values compared to non-printable formulations 3 and 4. As such, elastic moduli in the aforementioned range indicate suitable filament stiffness, which is beneficial for the purpose of printability, upon manual handling for feeding the printhead. Generally, elasticity appears to play a major role in filament printability, because filaments with very high elasticity are too soft to be printed (Form. 3 & 4) as they twine inside the printhead and filaments with very low elasticity are too stiff and have a tendency to break (Zhang et al., 2017). On the other hand, the hardness for formulations 3, 4, 7a, 7b, 8 is almost the same and at first sight does not provide any clear indication regarding printability. Though judging from the successful 3D printing of formulations 7a, 7b and 8, such hardness values, not necessarily excessively high as seen for formulation 1, make filaments less prone to localized damage that could lead to premature fracture by the feeding gears inside the printhead. Therefore, filaments produced with formulations 7a, 7b, and 8 appear more suitable for 3D printing, because they possess the appropriate combination of hardness and elastic moduli values.

SEM images of produced PVA-glimepiride filament (depicted in Fig. 5A) revealed a compact filament, with smooth surface, containing a small number of tiny pores. Images of Eudragit®-metformin filament produced in single-screw extruder (Fig. 5B), appeared to be also compact, although surface roughness was increased and tiny pores were still present. Finally, Eudragit®-metformin filament produced in twin-screw extruder presented high surface roughness and significant increase in internal porosity -Fig. 5C- (verified by the higher amount of filament needed to achieve the desired formulation mass, as presented in Eqs. (9) and (10)).

Moreover, SEM zoom-ins revealed the relatively smooth surface of the 3D printed PVA-based layer of the dosage forms (Fig. 6A), whereas in less magnified images, fusion between the 3D printed strands and the presence of scarce tiny pores between these strands can be observed (Fig. 6B). The images in Fig. 6C and D depict the areas of the 3D printed dosage forms where PVA-based and Eudragit® RL -based layers connect with each other. In these lateral images it can be observed that, in the case of 3D prints fabricated with single-screw produced filament, Eudragit®-based layers are clearly distinguishable (Fig. 6C), whereas in 3D prints fabricated with single-screw produced filament, Eudragit®-based layer appears as a relatively uniform rough mass (Fig. 6D). That roughness results in imperfections of the deposition of the PVA-based on the Eudragit® RL-based layer (tiny gaps be-

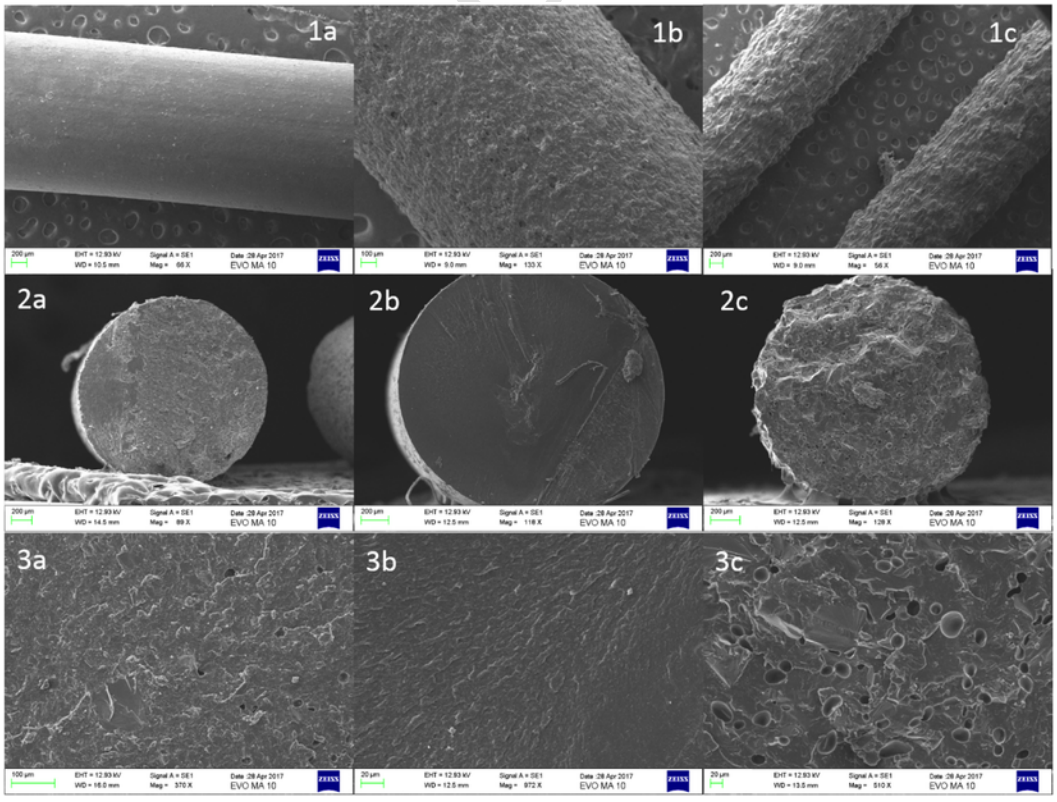

Fig. 5. SEM images (filaments (1), cross-sections (2) and surface zoom-ins (3)) of glimepiride-loaded PVA filament (a), metformin-loaded Eudragit® RL single-screw filament (b) and metformin-loaded Eudragit® RL twin-screw filament (c).

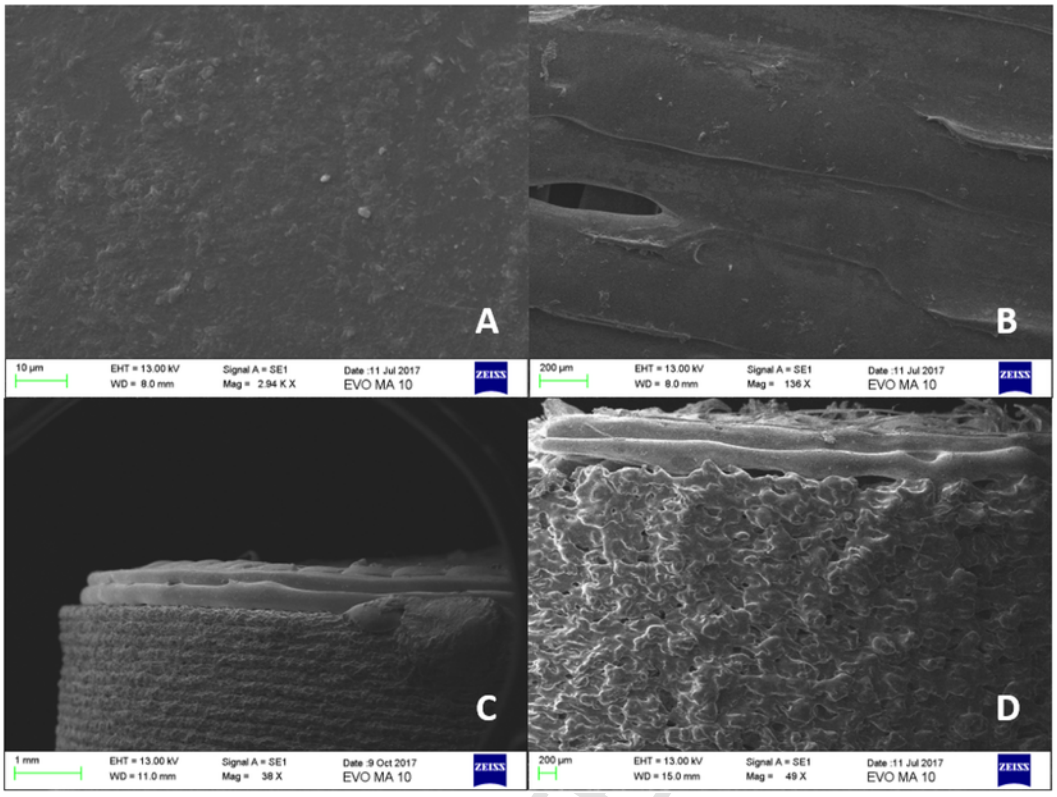

Fig. 6. SEM images of: A. glimepiride-loaded PVA 3D printed layer zoom-in, B. glimepiride-loaded PVA 3D printed layer, C. lateral view of 3D printed dosage form produced from single-screw filament and D. lateral view of 3D printed dosage form produced from single-screw filament.

tween the two layers). Nevertheless, these imperfections did not appear to compromise the structural integrity of these dosage forms macroscopically.

DSC thermograms are shown in Fig. 7. Pure glimepiride exhibits an endothermic peak at 217 °C (T_m), followed by gradual degradation (Cides et al., 2006). Mannitol exhibits a melting endothermic peak at 170 °C (Gombás et al., 2003), whereas Mowiol 4–88® melts completely at 195 °C, although this process starts earlier at about 165 °C, showing a behavior of a typical partially crystalline polymer (Pshezhetskii et al., 1990). Slight signal drop at the range 70-140 °C is associated with gradual loss of H_2O bound to the polymer and the small peak at 50–60 °C might be attributed to polymer's T_g value (Pshezhetskii et al., 1990). Calcium stearate exhibits a broad twin-peak endotherm ranging from 90 to 130 °C. The first peak (~112 °C) is attributed to the loss of crystallization water (calcium stearate is a monohydrate) and the second (~120 °C) to the collapse of the crystal lattice (crystalline-to-smectic phase). Also, two minor peaks observed at 152 °C and 190 °C, are attributed to the transitions between the smectic-to-nematic and the nematic-to-isotropic liquid phase respectively (Shi et al., 2010).

PVA-mannitol filament loaded with glimepiride shows a broad peak at 180 °C, corresponding to the melting of PVA, that appears to melt approximately 15 °C lower than pure Mowiol 4–88®. The suppression of T_m might be attributed to the presence of plasticizer (mannitol) in the polymer matrix (Baiardo et al., 2003). Melting peak of mannitol completely disappears, indicating its gradual dissolution in the molten polymer and complete conversion to the amorphous state (Liu et al., 2013). On the contrary, melting point of glimepiride appears at 180 °C, as a physical interaction with calcium stearate suppresses its melting point by ~35 °C (Cides et al., 2006). This physical interaction does not result in incompatibility, as IR spectra indicate no chemical interaction between glimepiride and calcium stearate (characteristic peaks present, according to literature (Cides et al., 2006)). The same interaction is also recorded in the DSC thermogram of the layer compounds' physical mixture. DSC thermogram of 3D printed PVA-mannitol-glimepiride layer appears to be identical to the corresponding filament thermogram.

DSC thermogram of PLA shows two endotherms at 64 °C and 150 °C, corresponding to polymer's glass transition and melting temperatures respectively and a broad exotherm between 85 and 135 °C, indicating PLA crystallization (Cao et al., 2003). Metformin's melting is present as a sharp endotherm peaking at 235 °C (Batra et al., 2017). Eudragit® RL PO presents glass transition at 62 °C and a broad endotherm between 145 and 220 °C, associated with gradual melt and subsequent degradation of the polymer (Parikh et al., 2014). All the above peaks are present in the physical mixture of the aforementioned substances (noting that T_m of metformin shifted slightly to 230 °C).

The predominant peak in DSC thermograms of metformin-Eudragit® RL-PLA-PEG 400 filament and 3D printed layer is the melting peak of metformin (slightly shifted at 227 °C), whereas PLA melting endotherm is also still visible at 150 °C. PLA crystallization exotherm has almost disappeared in both thermograms. Moreover, it should be mentioned that addition of plasticizer suppressed Tg of both polymers by ~10 °C.

TGA thermograms shown in Fig. 8 indicate that all the raw materials, the produced filaments and the 3D printed dosage forms, are stable at extrusion (140 °C–157 °C for Eudragit® filament and 190 °C for PVA filament) and printing temperatures (170 °C and 205 °C respectively).

Specifically, significant decomposition of mannitol was observed above 240 °C (mass loss at 200 °C was $<0.5\%$), whereas PVA appears to start decomposing at 220 °C (decomposition becomes rapid after 260 °C) in accordance with previous reports (Goyanes et al., 2015c). Finally, for glimepiride the onset of decomposition is observed after 212 °C (Cides et al., 2006). Mass losses of PVA and PVA containing entities (filament and 3D printed dosage form) observed at temperature

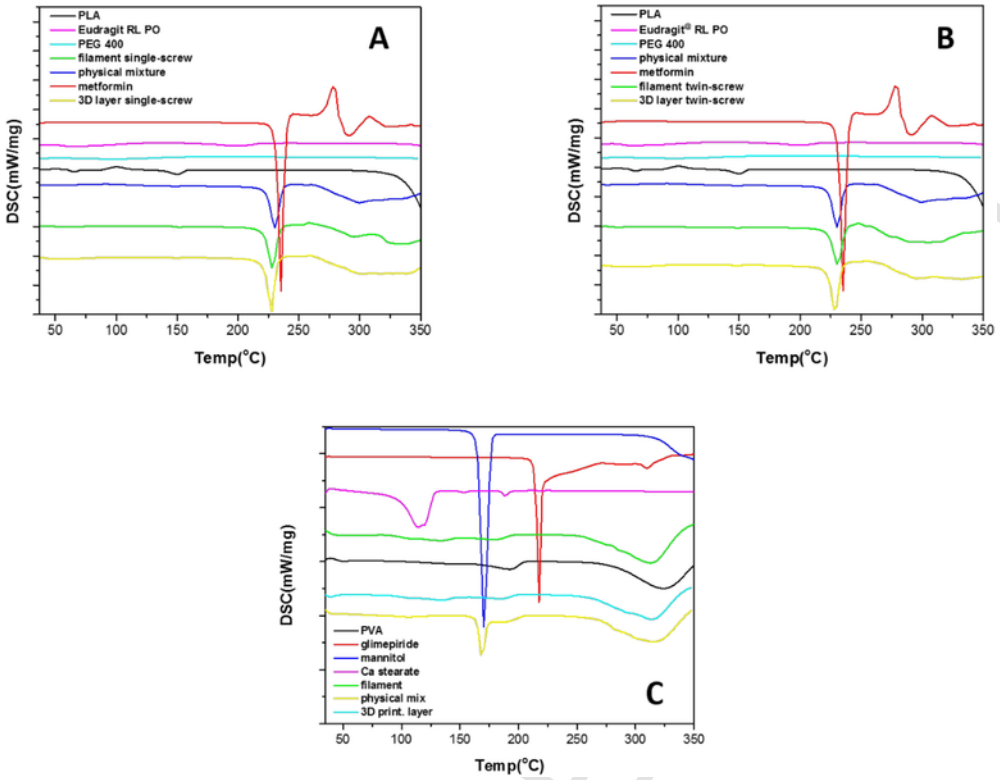

Fig. 7. DSC thermograms of API's, excipients, their physical mixtures, HME produced filaments and 3D printed formulations of: A. single-screw produced metformin-loaded layer, B. twin-screw produced metformin-loaded layer and C. glimepiride-loaded layer.

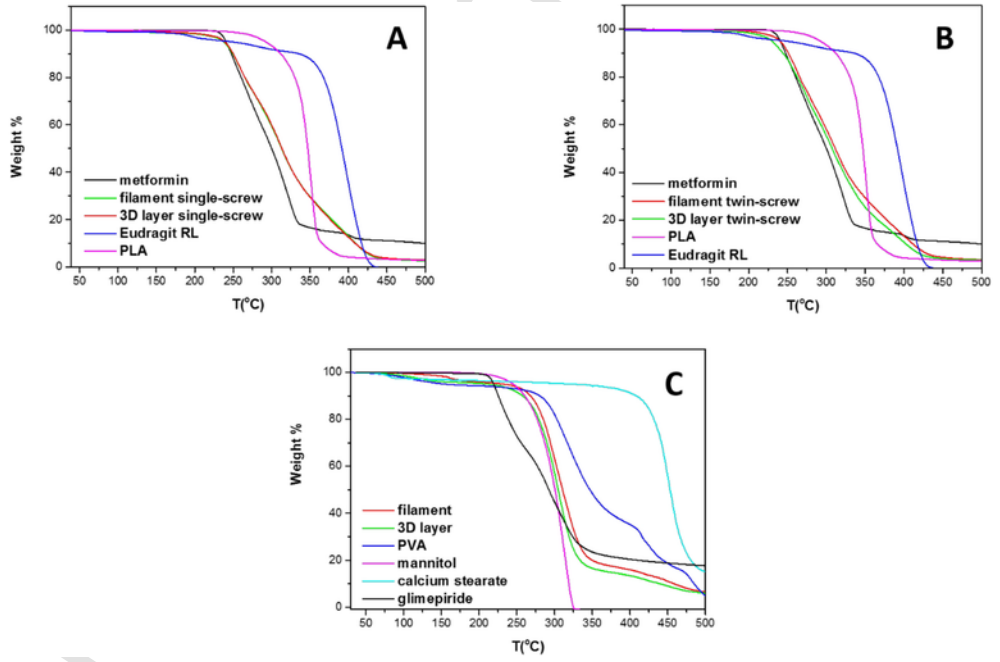

Fig. 8. TGA thermograms of API's, excipients, their physical mixtures, HME produced filaments and 3D printed formulations of: A. single-screw produced metformin-loaded layer, B. twin-screw produced metformin-loaded layer and C. glimepiride-loaded layer.

range 60–180 °C, might be attributed to the loss of absorbed water (about 3–5% w/w).

Metformin starts decomposing after melting (235 °C), with decomposition accelerating after 250 °C (Santos et al., 2008). Eudragit® RL PO is stable until 170 °C, where slow degradation procedure begins (Parikh et al., 2014), whereas PLA decomposes above 300 °C (Al-Itry et al., 2012).

XRD diffractograms of pure glimepiride and mannitol shown in Fig. 9 exhibit multiple distinct peaks, indicating their crystalline nature. Mannitol characteristic peaks correspond to beta-D-mannitol (CSD-DMANTL11), whereas glimepiride (CSD-TOHBUN01) main peaks

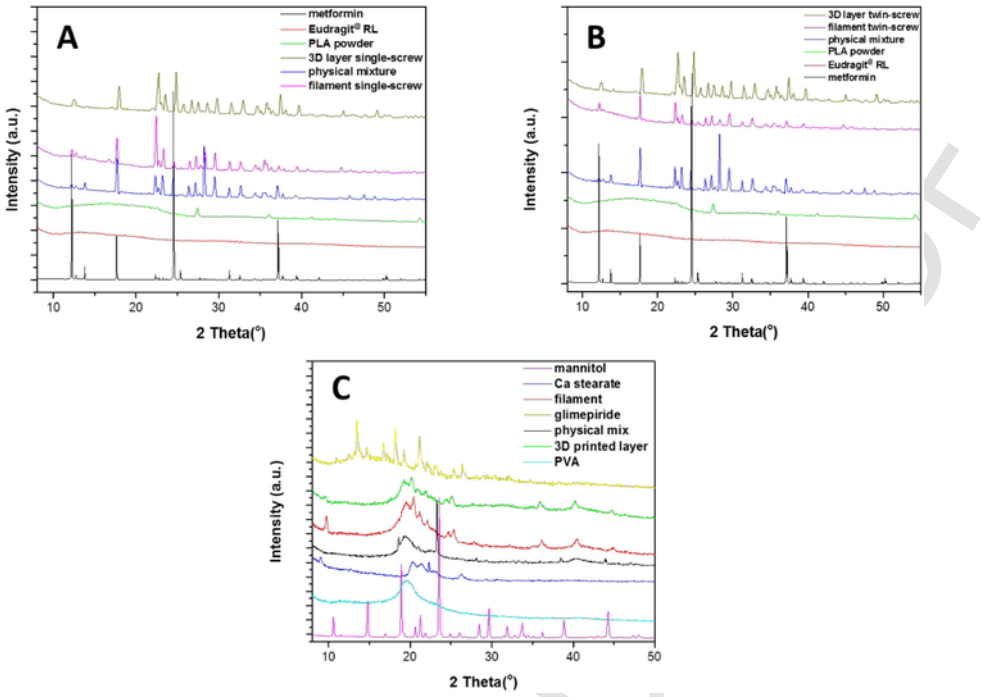

Fig. 9. XRD diagrams of API's, excipients, their physical mixtures, HME produced filaments and 3D printed formulations of: A. single-screw produced metformin-loaded layer, B. twin-screw produced metformin-loaded layer and C. glimepiride-loaded layer.

(13.52, 18.23, 21.18) correspond to polymorph I (Bonfilio et al., 2012; Nagpal et al., 2012). Glimepiride diffraction peaks disappear in PVA filament and 3D printed dosage form, indicating the conversion of the API to an amorphous dispersion inside the polymer matrix. That conversion can be beneficial, as amorphous dispersions facilitate solubilization of low solubility APIs, like glimepiride (Solanki et al., 2017). Also, XRD peaks of mannitol beta form are replaced from those corresponding to delta form, revealing the polymorphic transition of the plasticizer (Cares-Pacheco et al., 2014).

Metformin HCl seems to be present at its thermodynamically stable form A (CSD-JAMRYI01), showing predominant peaks at 12.2, 17.7, 24.42 and 37.11 (Vippagunta et al., 2010). Some of these peaks are present in HME filament and 3D printed Eudragit® RL layers, with significantly decreased intensity. That intensity suppression can be attributed to both dilution and partial loss of crystallinity of the API inside the polymer formulation.

Porosity analysis indicated a void/matrix volume ratio of 0.038 (0.64/16.99 μm^3); that is a porosity of 3.8%, and a median porous size of 87,502.75 μm^3. The results of the analysis are summarized in Table 3.

Structural and morphological characteristic such as percentage (%) porosity or pore-size distribution, play significant role on the performance of the manufactured dosage forms [Markl et al., 2017] as amongst others they can affect dissolution- and drug-release rates. μCT imaging and image-based analysis allowed for non-destructive assessment of the inner structure, quantification of the porosity characteristics and of the accuracy of the print. The 3D printed dosage form showed a level of porosity similar to that previously reported by our group [Gioumouxouzis et al., 2017] and is also in agreement with that previous reported by Markl et al., 2017 for 3D printed dosage forms made of PVA.

Figs. 10 and 11(A–D) show the deviation map of printed object's surface compared to the nominal values of the CAD design. The results show the deviation ranging from −100, +200 μm on the majority of the surface, with a small area of high-variation not exceeding ±500 μm. Fig. 10 shows that area of over-deposition of material, depicted as or-

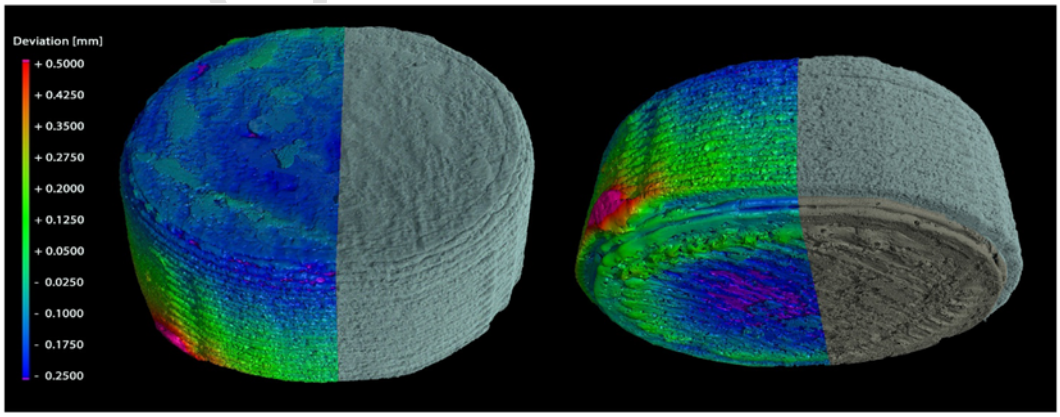

Fig. 10. [a & b]: Combined μCT and deviation map volume renderings showing the deviation from the CAD design with respect to each one of the deposited layers; i.e. Eudragit® (turquoise) and PVA (khaki-brown). (For interpretation of the references to color in this figure legend, the reader is referred to the web version of this article.)

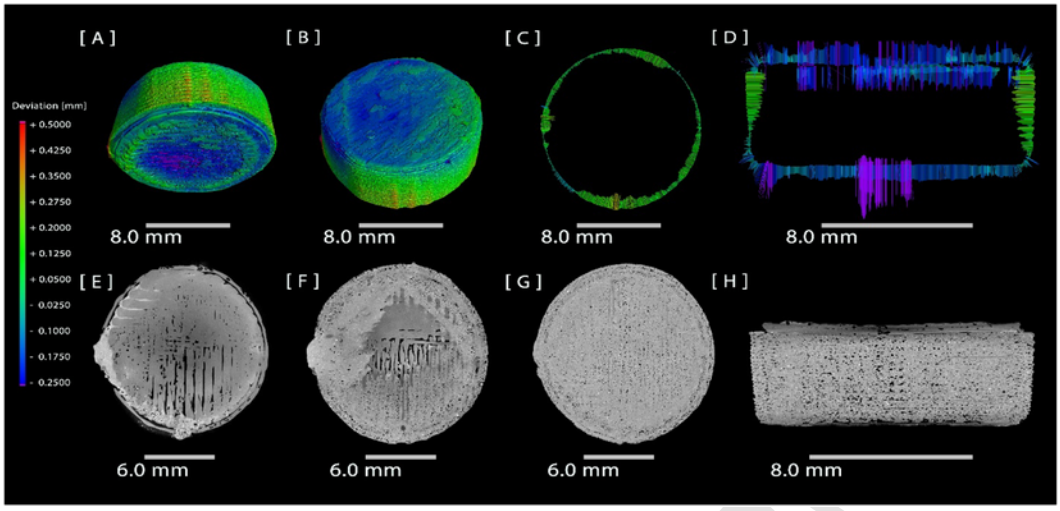

Fig. 11. [a & b]: Volume rendering of the printed object showing the deviation map of printed object's surface compared to the nominal values of the CAD design; [c & d]: deviation maps through the central XY and ZX slices of the object; [e -g]: XY CT slices showing virtual cross-sections taken at the centre of the PVA layer, the PVA/Eudragit® layer interface and the centre of the Eudragit® layer respectively; [h]: XY CT slices showing virtual cross-sections through the XZ plane of the object.

ange/red bands that signify increased deviation. The deviation of that spot is attributed to the brief immobilization of the first heated nozzle, during nozzle switch between Eudragit® and PVA layer creation, that results in deposition of a tiny amount of additional material.

Additionally, it can be observed that both top and bottom surfaces of the dosage form exhibit a slight "sinking" with direction from their edges to their central areas. That curvature of the object (biconcave), is attributed to the linear stop-and-reverse motion of the printing head, when infill of a layer is deposited. Moreover, that effect results in decreased porosity at the peripheral region of the dosage form, as more material is deposited there, in contrast to the central region (Fig. 11H).

The deviation increase that can be seen in the XY central slice in Fig. 11D, is due to the gradual increase of the diameter of the printed object. This can be better seen in Fig. 11H, which shows the equivalent CT XY central slice. That observable increase of the diameter of the dosage form with direction from bottom to top, can be attributed to the tendency of the molten printed material to spread out slightly, after being laid on the previous layer (i.e. the strands of the deposited material from the printhead are not perfect cylindrical rods, but elliptical). As a result, every layer expands slightly more than its underlying ones, as it has more space available to step onto (a "reverse-pyramid" effect). This could be problematic for printing larger objects, but it is sufficient for printing objects at the size of a pharmaceutical dosage form with acceptable accuracy.

Fig. 11(E, F and G) show XZ slices taken at the centre of the PVA layer, the PVA/Eudragit® layer interface and the centre of the Eudragit® layer respectively. The decrease in porous size of the latter can be observed and can be attributed to the different nature of the formulations, as PVA layer consists mainly of polymer (80%) that has a tendency to create long uniform cohesive strands that are, nevertheless, not always perfectly fused with each other, creating long macro-pores, whereas Eudragit® layer incorporates 50% API, resulting in rougher 3D printed surfaces, that fuse better with each other allowing the creation of only small micro-pores inside the formulation.

Dimensions, weights, drug loadings and their deviations from theoretical values are presented in Table 2 and images of a typical 3D printed dosage form in Fig. 11(A–D).

Friability tests were not conducted, since previous studies have demonstrated that FDM produced dosage forms exhibit zero friability and very high crushing strength (Gioumouxouzis et al., 2017; Goyanes et al., 2015a; Sadia et al., 2016). These results are supported by the fact that mechanical strength is an inherent property of FDM 3D printed structures (presenting tensile strength values >10 MPa, depending on the material used) (Wong and Hernandez, 2012), whereas pharmaceutical tablets are considered acceptable when having tensile strength 1.5–2.5 MPa (Podczeck, 2012).

Dissolution tests of bilayer pills (Fig. 12) revealed that, in the case of dosage forms deriving from filament produced with single-screw extruder, metformin dissolution was complete, as 100% of the API was dissolved after 480 min. Dosage forms produced from twin-screw extruder, showed slightly slower metformin release (91,76% after 540 min. and 86,98% after 480 min.). This delay of release could be attributed to slightly bigger size of these kind of dosage forms, in comparison to single-screw derived ones, that probably delays metformin release from Eudragit® matrix (Table 3).

The largest percentage (87.04%) of glimepiride from the upper immediate release layer was dissolved after 75 min. Glimepiride dissolution reached a plateau of 91.31% after 120 min. The deviation from theoretical 100% can be attributed to the height deviation of the layers from ideal layer height that resulted in dosage forms with slightly lighter PVA upper layer (and thus containing less glimepiride).

Eventually, it can be concluded that the formulations were successful, as the release of the API's was complete within the desirable absorption margins (2–3 h for glimepiride and 8 h for metformin) (Ning et al., 2011; Song, 2016; "USP39–NF34, Metformin Hydrochloride Extended-Release Tablets", 2016).

4. Conclusions

In the current work, a two-compartment antidiabetic formulation was developed using FDM 3D printing, that combines glimepiride (immediate release) and metformin (sustained release), making co-administration and once-daily dosing of the two regimens feasible. Evaluation of Hot-Melt extruded filaments used for 3D printing exhibited sufficient printability of filaments, regardless of the extruder used (twin-or single-screw), although the single-screw extruder produced more compact filaments, a result attributed to the higher pressure induced by the larger screw of the single-screw extruder. Dynamic Micro-Indentation Testing, enabled the mechanical characterization of the produced filaments at a more fundamental level than conventional techniques, revealing the hardness/elasticity values that indicate printable filaments. Morphological micro- and macro analysis of the 3D printed dosage forms, by means of μCT and SEM, revealed that their dimensions and internal structure were generally consistent to the computer designed

Table 2
Measured properties of 3D printed formulations (A) and (B) (n = 3 ± S.D.). % divergences of measured properties of 3D printed formulations (A) and (B) from theoretically targeted values.

Formulations	Diameter (mm)	Divergence %	Height (mm)	Divergence %	Printed dosage form weight (mg)	Divergence %	Metformin drug loading (mg)	Metformin drug loading %	Glimepiride drug loading (mg)	Glimepiride drug loading %
A (twin-screw)	14.98 ± 0.07	0.14	5.97 ± 0.07	1.97	1089 ± 8.72	2.46	458.80 ± 21.83	91.76	1.82 ± 0.1	91.06
B (single-screw)	15.09 ± 0.12	0.60	5.67 ± 0.13	1.05	1107.15 ± 17.13	0.84	504.37 ± 28.32	100.87	1.70 ± 0.05	85.24

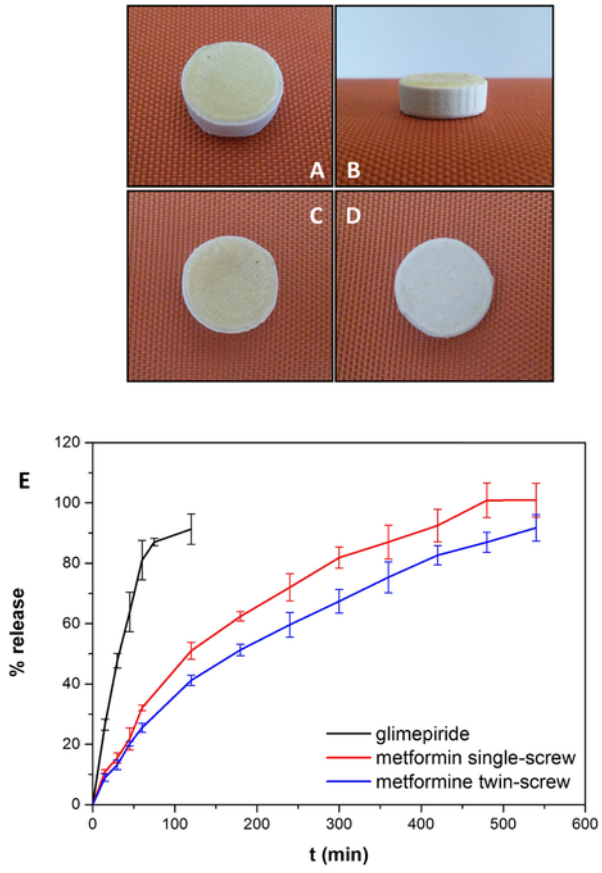

Fig. 12. Images of the 3D printed formulations: A. Front view, B. Side view, C. Top view, D. Bottom view. E. Dissolution curves of the API's from their 3D printed formulations (PVA matrix for glimepiride and Eudragit® RL matrix for metformin).

templates, ensuring acceptable drug-loading accuracy. Concluding, we demonstrated that FDM 3D printing is a promising technique for the fabrication of complex personalized medicines, incorporating API's with different desired release profiles, indicating the potentiality of a plethora of drug combinations that will revolutionize pharmacotherapy, reducing frequency of medication intake and ensure the administration of the exact drug dose determined for each individual patient.

Conflict of interest

The authors report no declarations of interest. This research did not receive any specific grant from funding agencies in the public, commercial, or not-for-profit sectors.

Uncited reference

Kyobula et al., 2017

Table 3
Results summary of the porosity analysis. "Volume" describes the distribution of pore sizes, "Surface" describes the distribution of the surface area of the pores and "Number of object voxels" describes the size/volume of the pores in the voxel domain. Analysis was conducted on 16.99 mm3 (253x253x251 voxels) central sub-volume in Fiji/ImageJ. The figures shown in this table are summarizing the analysis of 2813 pores/object.

	Mean	Standard deviation	SE of mean	Sum	Minimum	Median	Maximum
Volume (μm^3)	2.28E + 05	5.83E + 05	1.10E + 04	6.40E + 08	3.56E + 04	8.75E + 04	1.38E + 07
Surface (μm^2)	2.80E + 04	4.74E + 04	8.94E + 02	7.87E + 07	7.33E + 03	1.55E + 04	9.19E + 05
Number of object voxels	3.20E + 02	8.20E + 02	1.55E + 01	9.00E + 05	5.00E + 01	1.23E + 02	1.94E + 04

References

Abeykoon, C., Li, K., McAfee, M., Martin, P.J., Niu, Q., Kelly, A.L., Deng, J., 2011. A new model based approach for the prediction and optimisation of thermal homogeneity in single screw extrusion. Control. Eng. Pract. 19, 862–874. https://doi.org/10.1016/j.conengprac.2011.04.015.

Al-Itry, R., Lamnawar, K., Maazouz, A., 2012. Improvement of thermal stability, rheological and mechanical properties of PLA, PBAT and their blends by reactive extrusion with functionalized epoxy. Polym. Degrad. Stab. 1898–1914. https://doi.org/10.1016/j.polymdegradstab.2012.06.028.

Aydin, A.A., Ilberg, V., 2016. Effect of different polyol-based plasticizers on thermal properties of polyvinyl alcohol:starch blends. Carbohydr. Polym. 136, 441–448. https://doi.org/10.1016/j.carbpol.2015.08.093.

Baiardo, M., Frisoni, G., Scandola, M., Rimelen, M., Lips, D., Ruffieux, K., Wintermantel, E., 2003. Thermal and mechanical properties of plasticized poly(L-lactic acid). J. Appl. Polym. Sci. 90, 1731–1738. https://doi.org/10.1002/app.12549.

Batra, A., Desai, D., Serajuddin, A.T.M., 2017. Investigating the use of polymeric binders in twin screw melt granulation process for improving compactibility of drugs. J. Pharm. Sci. 106, 140–150. https://doi.org/10.1016/j.xphs.2016.07.014.

Beck, R.C.R., Chaves, P.S., Goyanes, A., Vukosavljevic, B., Buanz, A., Windbergs, M., Basit, A.W., Gaisford, S., 2017. 3D printed tablets loaded with polymeric nanocapsules: an innovative approach to produce customized drug delivery systems. Int. J. Pharm. 528, 268–279. https://doi.org/10.1016/j.ijpharm.2017.05.074.

BNF, 2014. BMJ Group and the Royal Pharmaceutical Society of Great Britain. 2014, 458–460.

Boetker, J., Water, J.J., Aho, J., Arnfast, L., Bohr, A., Rantanen, J., 2016. Modifying release characteristics from 3D printed drug-eluting products. Eur. J. Pharm. Sci. 90, 47–52. https://doi.org/10.1016/j.ejps.2016.03.013.

Bonfilio, R., Pires, S.A., Ferreira, L.M.B., de Almeida, A.E., Doriguetto, A.C., de Araújo, M.B., Salgado, H.R.N., 2012. A discriminating dissolution method for glimepiride polymorphs. J. Pharm. Sci. 101, 794–804. https://doi.org/10.1002/jps.22799.

Cao, X., Mohamed, A., Gordon, S.H., Willett, J.L., Sessa, D.J., 2003. DSC study of biodegradable poly(lactic acid) and poly(hydroxy ester ether) blends. Thermochim. Acta 406, 115–127. https://doi.org/10.1016/S0040-6031(03)00252-1.

Cares-Pacheco, M.G., Vaca-Medina, G., Calvet, R., Espitalier, F., Letourneau, J.J., Rouilly, A., Rodier, E., 2014. Physicochemical characterization of D-mannitol polymorphs: the challenging surface energy determination by inverse gas chromatography in the infinite dilution region. Int. J. Pharm. 475, 69–81. https://doi.org/10.1016/j.ijpharm.2014.08.029.

Chai, X., Chai, H., Wang, X., Yang, J., Li, J., Zhao, Y., Cai, W., Tao, T., Xiang, X., 2017. Fused deposition modeling (FDM) 3D printed tablets for intragastric floating delivery of domperidone. Sci. Rep. 7, 2829https://doi.org/10.1038/s41598-017-03097-x.

Cheng, C.L., Yu, L.X., Lee, H.L., Yang, C.Y., Lue, C.S., Chou, C.H., 2004. Biowaiver extension potential to BCS Class III high solubility-low permeability drugs: bridging evidence for metformin immediate-release tablet. Eur. J. Pharm. Sci. 22, 297–304. https://doi.org/10.1016/j.ejps.2004.03.016.

Cides, L.C.S., Araújo, A.A.S., Santos-Filho, M., Matos, J.R., 2006. Thermal behaviour, compatibility study and decomposition kinetics of glimepiride under isothermal and non-isothermal conditions. J. Therm. Anal. Calorim. 84, 441–445. https://doi.org/10.1007/s10973-005-7131-8.

Clariant, 1999. Mowiol® - polyvinyl alcohol. In: Sulzbach. pp. C1–C10.

Dissolution Methods, U.S. FDA. URL https://www.accessdata.fda.gov/scripts/cder/dissolution/dsp_getallData.cfm, (n.d., www document, accessed 6.25.17).

Genina, N., Hollander, J., Jukarainen, H., Makila, E., Salonen, J., Sandler, N., 2016. Ethylene vinyl acetate (EVA) as a new drug carrier for 3D printed medical drug delivery devices. Eur. J. Pharm. Sci. 90, 53–63. https://doi.org/10.1016/j.ejps.2015.11.005.

Gioumouxouzis, C.I., Katsamenis, O.L., Bouropoulos, N., Fatouros, D.G., 2017. 3D printed oral solid dosage forms containing hydrochlorothiazide for controlled drug delivery. J. Drug Deliv. Sci. Technol. 40, 164–171. https://doi.org/10.1016/j.jddst.2017.06.008.

Gombás, , Szabó-Révész, P., Regdon, G., Erös, I., 2003. Study of thermal behaviour of sugar alcohols. J. Therm. Anal. Calorim. 615–621. https://doi.org/10.1023/A:1025490432142.

Goyanes, A., Buanz, A.B.M., Hatton, G.B., Gaisford, S., Basit, A.W., 2015. 3D printing of modified-release aminosalicylate (4-ASA and 5-ASA) tablets. Eur. J. Pharm. Biopharm. 89, 157–162. https://doi.org/10.1016/j.ejpb.2014.12.003.

Goyanes, A., Chang, H., Sedough, D., Hatton, G.B., Wang, J., Buanz, A., Gaisford, S., Basit, A.W., 2015. Fabrication of controlled-release budesonide tablets via desktop (FDM) 3D printing. Int. J. Pharm. 496, 414–420. https://doi.org/10.1016/j.ijpharm.2015.10.039.

Goyanes, A., Robles Martinez, P., Buanz, A., Basit, A.W., Gaisford, S., 2015. Effect of geometry on drug release from 3D printed tablets. Int. J. Pharm. 494, 657–663. https://doi.org/10.1016/j.ijpharm.2015.04.069.

Goyanes, A., Wang, J., Buanz, A., Martinez-Pacheco, R., Telford, R., Gaisford, S., Basit, A.W., 2015. 3D printing of medicines: engineering novel oral devices with unique design and drug release characteristics. Mol. Pharm. 12, 4077–4084. https://doi.org/10.1021/acs.molpharmaceut.5b00510.

Holländer, J., Genina, N., Jukarainen, H., Khajeheian, M., Rosling, A., Mäkilä, E., Sandler, N., 2016. Three-dimensional printed PCL-based implantable prototypes of medical devices for controlled drug delivery. J. Pharm. Sci. 105, 2665–2676. https://doi.org/10.1016/j.xphs.2015.12.012.

Hwang, Y.C., Kang, M., Ahn, C.W., Park, J.S., Baik, S.H., Chung, D.J., Jang, H.C., Kim, K.A., Lee, I.K., Min, K.W., Nam, M., Park, T.S., Son, S.M., Sung, Y.A., Woo, J.T., Park, K.S., Lee, M.K., 2013. Efficacy and safety of glimepiride/metformin sustained release once daily vs. glimepiride/metformin twice daily in patients with type 2 diabetes. Int. J. Clin. Pract. 67, 236–243. https://doi.org/10.1111/ijcp.12071.

Khaled, S.A., Burley, J.C., Alexander, M.R., Yang, J., Roberts, C.J., 2015. 3D printing of five-in-one dose combination polypill with defined immediate and sustained release profiles. J. Control. Release 217, 308–314. https://doi.org/10.1016/j.jconrel.2015.09.028.

Khaled, S.A., Burley, J.C., Alexander, M.R., Yang, J., Roberts, C.J., 2015. 3D printing of tablets containing multiple drugs with defined release profiles. Int. J. Pharm. 494, 643–650. https://doi.org/10.1016/j.ijpharm.2015.07.067.

Kyobula, M., Adedeji, A., Alexander, M.R., Saleh, E., Wildman, R., Ashcroft, I., Gellert, P.R., Roberts, C.J., 2017. 3D inkjet printing of tablets exploiting bespoke complex geometries for controlled and tuneable drug release. J. Control. Release 261, 207–215. https://doi.org/10.1016/j.jconrel.2017.06.025.

Liu, J., Cao, F., Zhang, C., Ping, Q., 2013. Use of polymer combinations in the preparation of solid dispersions of a thermally unstable drug by hot-melt extrusion. Acta Pharm. Sin. B 3, 263–272. https://doi.org/10.1016/j.apsb.2013.06.007.

Mansour, G., Tzetzis, D., 2013. Nanomechanical characterization of hybrid multiwall carbon nanotube and fumed silica epoxy nanocomposites. Polym.-Plast. Technol. Eng. 52, 1054–1062. https://doi.org/10.1080/03602559.2013.769581.

Mansour, G., Tzetzis, D., Bouzakis, K.D., 2013. A nanomechanical approach on the measurement of the elastic properties of epoxy reinforced carbon nanotube nanocomposites. Tribol. Ind. 35, 190–199.

Markl, D., Zeitler, J.A., Rasch, C., Michaelsen, M.H., Müllertz, A., Rantanen, J., Rades, T., Bøtker, J., 2017. Analysis of 3D prints by X-ray computed microtomography and terahertz pulsed imaging. Pharm. Res. 34, 1037–1052. https://doi.org/10.1007/s11095-016-2083-1.

Maroni, A., Melocchi, A., Parietti, F., Foppoli, A., Zema, L., Gazzaniga, A., 2017. 3D printed multi-compartment capsular devices for two-pulse oral drug delivery. J. Control. Release 268, 10–18. https://doi.org/10.1016/j.jconrel.2017.10.008.

McCreight, L.J., Bailey, C.J., Pearson, E.R., 2016. Metformin and the gastrointestinal tract. Diabetologia https://doi.org/10.1007/s00125-015-3844-9.

Melocchi, A., Parietti, F., Loreti, G., Maroni, A., Gazzaniga, A., Zema, L., 2015. 3D printing by fused deposition modeling (FDM) of a swellable/erodible capsular device for oral pulsatile release of drugs. J. Drug Deliv. Sci. Technol. 30, 360–367. https://doi.org/10.1016/j.jddst.2015.07.016.

Nagpal, M., Nagpal, K., Singh, S., Rajera, R., Rakha, P., Mishra, D., 2012. Dissolution enhancement of glimepiride using modified gum karaya as a carrier. Int. J. Pharm. Investig. 2, 42. https://doi.org/10.4103/2230-973X.96925.

Ning, X., Sun, J., Han, X., Wu, Y., Yan, Z., Han, J., He, Z., 2011. Strategies to improve dissolution and oral absorption of glimepiride tablets: solid dispersion versus micronization techniques. Drug Dev. Ind. Pharm. 37, 727–736. https://doi.org/10.3109/03639045.2010.538061.

Okwuosa, T.C., Pereira, B.C., Arafat, B., Cieszynska, M., Isreb, A., Alhnan, M.A., 2016. Fabricating a shell-core delayed release tablet using dual FDM 3D printing for patient-centred therapy. Pharm. Res.1–11. https://doi.org/10.1007/s11095-016-2073-3.

Okwuosa, T.C., Stefaniak, D., Arafat, B., Isreb, A., Wan, K.W., Alhnan, M.A., 2016. A lower temperature FDM 3D printing for the manufacture of patient-specific immediate release tablets. Pharm. Res. 33, 2704–2712. https://doi.org/10.1007/s11095-016-1995-0.

Paes, A.H.P., Barker, A., Soe-Agnie, C.J., 1997. Impact of dosage frequency on patient compliance. Diabetes Care 20, 1512–1517. https://doi.org/10.2337/diacare.20.10.1512.

Parikh, T., Gupta, S.S., Meena, A., Serajuddin, A.T.M., 2014. Investigation of thermal and viscoelastic properties of polymers relevant to hot melt extrusion - III: Polymethacrylates and polymethacrylic acid based polymers. J. Excipients Food Chem. 5, 56–64. https://doi.org/10.1208/s12249-015-0426-6.

Pawar, Shraddha P., Meshram, Gangadhar A., Phadke, Manisha U., 2008. Simultaneous LC estimation of glimepiride and metformin in glimepiride immediate release and metformin sustained release tablets. Chromatographia 68, 1063–1066. https://doi.org/10.1365/s10337-008-0802-40009-5893/08/12.

Pietrzak, K., Isreb, A., Alhnan, M.A., 2015. A flexible-dose dispenser for immediate and extended release 3D printed tablets. Eur. J. Pharm. Biopharm. 96, 380–387. https://doi.org/10.1016/j.ejpb.2015.07.027.

Podczeck, F., 2012. Methods for the practical determination of the mechanical strength of tablets - from empiricism to science. Int. J. Pharm. https://doi.org/10.1016/j.ijpharm.2012.06.059.

Pshezhetskii, V.S., Rakhnyanskaya, A.A., Gaponenko, I.M., Nalbandyan, Yu.E., 1990. A differential scanning calorimetry study of polyvinyl alcohol. Polym. Sci. U.S.S.R. 32, 722–726.

Ramesh, D., Habibuddin, M., 2014. Stability indicating RP-HPLC method for the simultaneous determination of atorvastatin calcium, metformin hydrochloride, and glimepiride in bulk and combined tablet dosage form. Int. Sch. Res. Not. 2014, 1–8. https://doi.org/10.1155/2014/754695.

Rauwendaal, C., 2014. Polymer extrusion: fifth edition. In: Polymer Extrusion, Fifth edition, pp. 1–934. https://doi.org/10.3139/9781569905395.003.

Sadia, M., Sośnicka, A., Arafat, B., Isreb, A., Ahmed, W., Kelarakis, A., Alhnan, M.A., 2016. Adaptation of pharmaceutical excipients to FDM 3D printing for the fabrication of patient-tailored immediate release tablets. Int. J. Pharm. 513, 659–668. https://doi.org/10.1016/j.ijpharm.2016.09.050.

Sandler, N., Salmela, I., Fallarero, A., Rosling, A., Khajeheian, M., Kolakovic, R., Genina, N., Nyman, J., Vuorela, P., 2014. Towards fabrication of 3D printed medical devices to prevent biofilm formation. Int. J. Pharm. 459, 62–64. https://doi.org/10.1016/j.ijpharm.2013.11.001.

Santos, A.F.O., Basílio, I.D., De Souza, F.S., Medeiros, A.F.D., Pinto, M.F., De Santana, D.P., MacÊdo, R.O., 2008. Application of thermal analysis in study of binary mix-

tures with metformin. J. Therm. Anal. Calorim. 93, 361–364. https://doi.org/10.1007/s10973-007-7876-3.
Schilling, S.U., Bruce, C.D., Shah, N.H., Malick, A.W., McGinity, J.W., 2008. Citric acid monohydrate as a release-modifying agent in melt extruded matrix tablets. Int. J. Pharm. 361, 158–168. https://doi.org/10.1016/j.ijpharm.2008.05.035.
Schindelin, J., Arganda-Carreras, I., Frise, E., Kaynig, V., Longair, M., Pietzsch, T., Preibisch, S., Rueden, C., Saalfeld, S., Schmid, B., Tinevez, J.-Y., White, D.J., Hartenstein, V., Eliceiri, K., Tomancak, P., Cardona, A., 2012. Fiji: an open-source platform for biological-image analysis. Nat. Methods 9, 676–682. https://doi.org/10.1038/nmeth.2019.
Schneider, C.A., Rasband, W.S., Eliceiri, K.W., 2012. NIH image to ImageJ: 25 years of image analysis. Nat. Methods 9, 671–675. https://doi.org/10.1038/nmeth.2089.
Seymour, B.R., 1990. Polymeric Composites. VSP, Utrecht, 33.
Shi, X., Rosa, R., Lazzeri, A., 2010. On the coating of precipitated calcium carbonate with stearic acid in aqueous medium. Langmuir 26, 8474–8482. https://doi.org/10.1021/la904914h.
Song, R., 2016. Mechanism of metformin: a tale of two sites. Diabetes Care https://doi.org/10.2337/dci15-0013.
Solanki, N., Tahsin, M., Shah, A., Serajuddin, A.T.M., 2017. Formulation of 3D printed tablet for rapid drug release by fused deposition modeling (FDM): screening polymers for drug release, drug-polymer miscibility and printability. J. Pharm. Sci. https://doi.org/10.1016/j.xphs.2017.10.021.
Stationery Office (Great Britain), 2016. British pharmacopoeia 2016. URL http://biblioteca.corpmontana.com/dspace/handle/montana/4208, (www document, accessed 6.25.17).
Tzetzis, D., Mansour, G., Tsiafis, I., Pavlidou, E., 2013. Nanoindentation measurements of fumed silica epoxy reinforced nanocomposites. J. Reinf. Plast. Compos. 32, 160–173. https://doi.org/10.1177/0731684412463978.
US-
P39–NF34,
2016 USP39–NF34, Metformin Hydrochloride Extended-Release Tablets, 20164766.
Vippagunta, R.R., LoBrutto, R., Pan, C.K., Lakshman, J.P., 2010. Investigation of metformin HCl lot-to-lot variation on flowability differences exhibited during drug product processing. J. Pharm. Sci. 99, 5030–5039. https://doi.org/10.1002/jps.22207.
Wong, K.V., Hernandez, A., 2012. A review of additive manufacturing. ISRN Mech. Eng. 2012, 1–10. https://doi.org/10.5402/2012/208760.
Yalkowsky, S.H., He, Y., Jain, P., 2010. Handbook of Aqueous Solubility Data. CRC Press.
Zhang, J., Feng, X., Patil, H., Tiwari, R.V., Repka, M.A., 2017. Coupling 3D printing with hot-melt extrusion to produce controlled-release tablets. Int. J. Pharm. 519, 186–197. https://doi.org/10.1016/j.ijpharm.2016.12.049.